Electrospinning Preparation, Structure, and Photoluminescence Properties of $YBO_3:Eu^{3+}$ Nanotubes and Nanowires

Hongwei Song,*[,†,‡] HongQuan Yu,[†] Guohui Pan,[†] Xue Bai,[†] B. Dong,[†] X.T Zhang,[‡] and S. K. Hark*[,‡]

State Key Laboratory on Integrated Optoelectronics, College of Electronic Science and Engineering, Jilin University, Changchun 130012, P. R. China, and Department of Physics, The Chinese University of Hong Kong, Shatian, Hong Kong, P. R. China

Received March 17, 2008

A novel method, electrospinning, was explored to prepare europium-doped YBO_3 nanocrystalline phosphors. Narrow and size-controllable YBO_3 nanotubes and nanowires were obtained, varying from 40 to 500 nm. The average wall thickness of the nanotubes was only 5−10 nm. The structural properties were characterized by X-ray diffraction (XRD), Fourier-transform infrared absorption (FTIR), electron spin resonance (ESR), field emission scanning electron micrographs (FE-SEM), and high-resolution transmission electron micrographs (HR-TEM). The results indicate that theYBO_3 nanotubes and nanowires were hexangular in phase and single crystals or polycrystalline in structure. Some surface dangling bonds caused by transition metal ions lead to a change of the coordination number of boron from +3 to +4. The photoluminescent properties of the YBO_3: Eu^{3+} nanowires and nanotubes were also characterized. It was observed that the charge-transfer excitation bands of Eu^{3+} in the nanowires and nanotubes blue-shifted in contrast to those in bulk, because of the variation of coordination environments.

Introduction

As is well-known, the reduction of particle size of crystalline system results in important modification of their photoluminescence properties, due to its special electronic properties, such as the increase of surface to volume ratio and quantum confinement effects.[1,2] Rare earth (RE) compounds were extensively applied to lighting, field-emission display (FED), cathode ray tubes (CRT), and plasma display panel (PDP), thus the corresponding nanosized phosphors have attracted extensive attention.[3–5] It is expected that the nanosized phosphors can improve not only the luminescence quantum yield, but also the resolution of display. Up to now, a large number of rare-earth doped inorganic nanophosphors have been prepared and studied, including oxides,[6,7] sulfides,[8,9] and fluorides.[10,11] Among them, the oxide compounds are attracting the most interest, because of their favorable physical properties, such as good chemical stability and strong absorption in vacuum ultraviolet (VUV) and ultraviolet (UV) regions.

The optical properties of nanomaterials depend not only on the particle size but also on the morphology and structure of the nanocrystals.[12] In recent years, one-dimensional nanophosphors, such as nanowires and nanotubes, have attracted intense interests in both fundamental and applied studies.[13–15] They not only can play a crucial role in important future optoelectronic devices,[14,16] data storage,[17] and biochemical and chemical sensors[18] but also can be used to enrich our understanding of basic quantum mechanics. To date, various rare earth (RE) insulated one-dimensional oxide phosphors have been prepared and studied.[19–25]

* Corresponding author. E-mail: hwsong2005@yahoo.com.cn (H.S.); skhark@phy.cuhk.edu.hk (S.K.H.). Fax and Tel.: 86-431-86176320(H.S.).
† Jilin University.
‡ The Chinese University of Hong Kong.

(1) Trave, A.; Buda, F.; Fasolino, A. *Phys. Rev. Lett.* **1996**, *77*, 5405.
(2) Agger, J. R.; Anderson, M. W.; Pemble, E. M.; Terasaki, O.; Nozue, Y. *J. Phys. Chem. B* **1998**, *102*, 3345.
(3) Bhargava, R. N.; Gallagher, D.; Numikko, A. *Phys. Rev. Lett.* **1994**, *72*, 416.
(4) Yu, J. Q.; Liu, H.; Wang, Y.; Fernandez, F. E.; Jia, W.; Sun, L.; Jin, C.; Li, D.; Liu, J.; Huang, S. *Opt. Lett.* **1997**, *22*, 913.
(5) Qadra, S. B.; Skelton, E. F.; Hsu, D. *Phys. Rev. B* **1999**, *60*, 9194.
(6) Eilers, H.; Tissue, B. M. *Chem. Phys. Lett.* **1996**, *251*, 74.
(7) Ghosh, P.; Patra, A. *Langmuir* **2006**, *22*, 6321.
(8) Chowdhury, P. S.; Patra, A. *Phys. Chem. Chem. Phys.* **2006**, *8*, 1329.
(9) Chen, W.; Malm, J. Q.; Zwiller, V.; Huang, Y.; Liu, S.; Wallenberg, R.; Bovin, J. Q.; Samuelson, L. *Phys. Rev. B* **2000**, *61*, 11021.
(10) Martin, N.; Boutinaud, P.; Mabiou, R.; Cousseins, J. C.; Bouderbala, M. *J. Mater. Chem.* **1999**, *9*, 125.
(11) Heer, S.; Kömpe, K.; Gudel, H. U.; Haase, M. *Adv. Mater.* **2004**, *16*, 2012.
(12) Song, H. W.; Yu, L. X.; Lu, S. Z.; Wang, T.; Liu, Z.; Yang, L. M. *Appl. Phys. Lett.* **2004**, *85*, 470.
(13) Lijima, S. *Nature.* **1991**, *354*, 56.
(14) Daun, X. F.; Huang, Y.; Cui, Y.; Wang, J. F.; Lieber, C. M. *Nature* **2001**, *409*, 66.
(15) Dickey, E. C.; Crimes, C. A.; Jain, M. K.; Ong, K. G.; Qian, D.; Kichambare, P. D.; Andrews, R.; Jacques, D. *Appl. Phys. Lett.* **2001**, *79*, 4022.
(16) Kind, H.; Yan, H.; Law, M.; Messer, B.; Yang, P. *Adv. Mater.* **2002**, *14*, 158.
(17) Kong, Y. C.; Yu, D. P.; Zhang, B.; Fang, W.; Feng, S. Q. *Appl. Phys. Lett.* **2001**, *78*, 4.
(18) Cui, Y.; Wei, Q.; Park, H.; Lieber, C. M. *Science* **2003**, *299*, 1874.
(19) Meyssamy, H.; Riwotzki, K.; Kornowski, A.; Naused, S.; Haase, M. *Adv. Mater.* **1999**, *11*, 840.
(20) Yada, M.; Mihara, M.; Mouri, S.; Kijima, T. *Adv. Mater.* **2002**, *14*, 309.
(21) Wen, F.; Zhao, X.; Huo, H.; Chen, J.; Lin, E.; Zhang, J. *Mater. Lett.* **2002**, *55*, 152.
(22) Lin, J.; Huang, Y.; Zhang, J.; Song, H.; Elssfah, E.; Liu, S.; Luo, J.; Ding, X.; Qi, S.; Tang, C. *Appl. Phys. Lett.* **2006**, *89*, 033318.
(23) Ma, L.; Chen, C.; Zhao, J.; Zheng, Y. *J. Cryst. Growth.* **2007**, *303*, 590.
(24) Yu, L.; Li, D.; Yue, M.; Yao, J.; Lu, S. *Chem. Phys.* **2006**, *326*, 478.

10.1021/cm8007864 CCC: $40.75
Published on Web 06/19/2008

Bulk $YBO_3:Eu^{3+}$ is an efficient red phosphor widely used in PDP, which owns high UV transparency, exceptional optical damage threshold, and high quantum yield under VUV excitation.[26] The corresponding nanocrystals have been prepared by various wet-chemical techniques such as the hydrothermal method, the sol−gel method, etc.[27–30] Through these techniques, only inhomogeneous nanoparticles or microsized particles composed of one-dimensional nanounits (nanowires, nanotubes and nanobelts) were obtained. It is still a challenge to obtain uniformly dispersed one-dimensional nanostructures because the nanounits of YBO_3 have the tendency to aggregate. It is important to develop an approach to synthesizing one-dimensional YBO_3 structures to meet the demands of optical devices.

Electrospinning is a simple, versatile, and useful technique for fabricating nanofibers that are exceptionally long in length and uniform in diameter from a rich variety of functional materials.[31–33] The diameters of fibers prepared by this method can range from tens of nanometers to several micrometers. The morphology of the electrospinning fibers depends on the solvent and the solution properties, as well as on other processing variables. Recently, we developed this technique to prepare lanthanide oxide nanowires as well as composite nanowires of organic−RE complex compounds.[34] In this paper, we present the electrospinning preparation and structural and photoluminescence properties of YBO_3: Eu^{3+} nanowires and nanotubes. To the best of our knowledge, singly distributed and size-controllable one-dimensional $YBO_3:Eu^{3+}$ nanowires and nanotubes have not been reported until now. The diameter of the nanotubes prepared in this work approaches 40 nm, and the average thickness of the walls is only 5−10 nm. It is not usual to obtain such a small diameter from nanofibers prepared by electrospinning. Systemic studies on the dependence of photoluminescence properties of RE on the structure, size, and morphology in one-dimensional nanomaterials are also significant.

Experimental Section

(A) Sample Preparation. In the preparation of precursor solutions, 0.02 mol of yttrium acetate, 1.0×10^{-3} mol of europium acetate (1:0.05 in mole ratio), and 0.09 mol boric acid were dissolved in a mixed solvent composed of 1.2 mol acetic acid and 300 mL of deionized water. Appropriate amounts of the above precursor solutions were then added into a 10 wt % polyvinyl alcohol (PVA) solution at different ratios, followed by vigorous stirring in a water bath for 4 h at 50 °C to obtain the final electrospinning solutions.

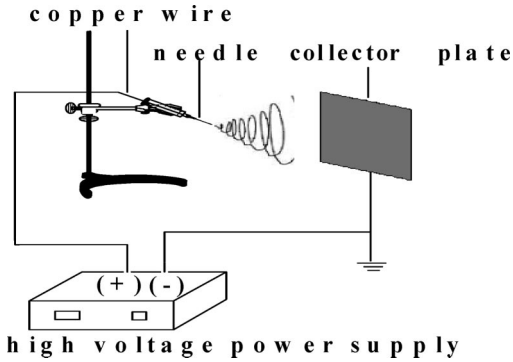

Figure 1. Schematic diagram of the electrospinning setup.

Figure 1 shows a schematic diagram of the electrospinning setup. It consists of three major components: a high-voltage power supply, a spinneret (a plastic needle), and a collector plate (a grounded conductor). In a typical electrospinning process, a precursor solution is ejected from the tip of spinneret under the effect of high-voltage that is applied between the spinneret and collector to form an electrically charged jet of solution. The solution jet solidified with accompanying evaporation of solvent and formed a nonwoven fibrous mat on the collector.

The precursor fibers of $YBO_3:Eu^{3+}$ were obtained by electrospinning with a distance of 5−25 cm between the spinneret tip and the collector and an applied voltage of 5−20 kV under the protection of a N_2 stream. The precursor fibers of $YBO_3:Eu^{3+}$ were dried initially for 12 h at room temperature under a vacuum, and were then annealed by heating from room temperature to 750 °C/min and kept for 1 h at 750 °C. After calcination, $YBO_3:Eu^{3+}$ nanowires or nanotubes were obtained. For comparison, bulk YBO_3: Eu^{3+} powders (Y:Eu = 1:0.05 in molar ratio) were also prepared by the method of solid-state reaction at 1100 °C for 8 h.

(B) Measurements. The XRD data of the fibers and bulk were collected on a Rigaku D/max-rA X-ray diffractometer, using a monochromatized Cu target radiation source ($\lambda = 1.5405$ Å). Scans were made from 15 to 65° (2θ) at a speed of 2° min^{-1}. FE-SEM images were obtained on a Hitachi S4800 field emission scanning electron microscope. The TEM images, HR-TEM images, selected area electron diffraction (SAED), and fast Fourier transform (FFT) images of the HR-TEM images were recorded on a JEM-3010 transmission electron microscope under a working voltage of 300 kV. The FTIR spectra were recorded on a FTS-3000 Bio-Rad spectrophotometer. The ESR spectra were measured by a GAES-FE3AX ESR spectrometer with a central magnetic field strength of 3366 G and scanning scope of 1000 G that was calibrated with DPPH.

The general excitation and emission spectra were recorded on a Hitachi F-4500 spectrophotometer equipped with a 150 W Xe-arc lamp at room temperature, and for comparison of different samples, the emission spectra were measured at a fixed band-pass of 0.2 nm with the same instrument parameters (2.5 nm for excitation slit, 2.5 nm for emission slit and 700 V for PMT voltage). In the measurements of time-resolved emission spectra and fluorescence dynamics, the 266 nm light from a fourth-harmonic-generator pumped by a pulsed Nd: YAG laser, was used as excitation source. The Nd: YAG laser had a line width of 0.3 cm^{-1}, pulse duration of 10 ns and repetition frequency of 10 Hz. A Spex 1403 spectrometer, a photon-multiplier and a boxcar integrator were used for the detection of the spectra. Fluorescence dynamics were recorded by a TEKTRONIX TDS-3052 oscilloscope. In the measurements of temperature-dependence of fluorescence, the

(25) Song, H. W.; Yu, L. X.; Yang, L. M.; Lu, S. Z. *J. Nanosci. Nanotechnol.* **2005**, *5*, 1519.
(26) Wegh, R. T.; Donker, H.; Oskam, K. D.; Meijerink, A. *Science* **1999**, *283*, 663.
(27) Jiang, X.; Yan, C.; Sun, L.; Wei, Z.; Liao, C. *J. Solid State Chem.* **2003**, *175*, 245.
(28) Wei, Z.; Sun, L.; Liao, C.; Yin, J.; Jiang, X.; Yan, C. *Appl. Phys. Lett.* **2002**, *80*, 1447.
(29) Pan, G. H.; Song, H. W.; Yu, L. X.; Liu, Z. X.; Lei, Y. Q.; Fan, L. B.; Lu, S. Z.; Ren, X. G. *J. Nanosci. Nanotechnol.* **2007**, *7*, 593.
(30) Zhang, J.; Lin, J. *J. Cryst. Growth* **2004**, *271*, 207.
(31) Caruso, R. A.; Schattka, J. H.; Greiner, A. *Adv. Mater.* **2001**, *13*, 1577.
(32) Li, D.; Xia, Y. *Adv. Mater.* **2004**, *16*, 1151.
(33) Li, D.; Ou, G.; Xia, Y. *Nano. Lett.* **2005**, *5*, 913.
(34) Yu, H. Q.; Song, H. W.; Pan, G. H.; Fan, L.; Li, S.; Bai, X.; Zhao, H. *J. Lumin.* **2007**, *124*, 39.

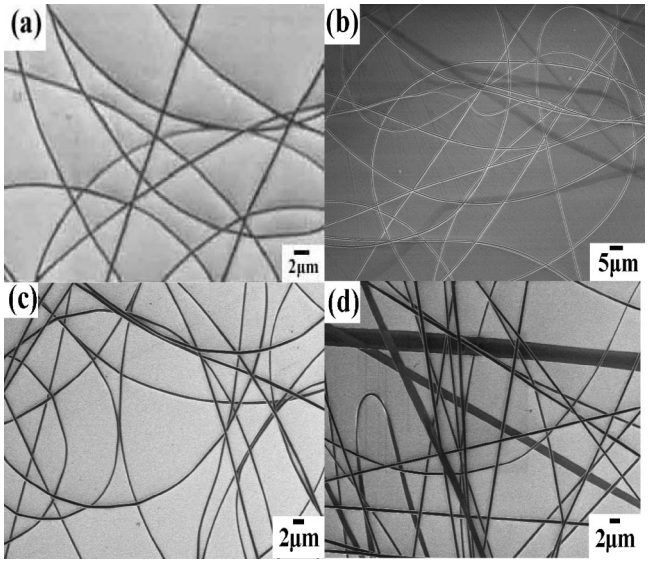

Figure 2. FE-SEM images of the precursors fibers of $YBO_3:Eu^{3+}$ prepared at different applied voltages: (a) 5, (b) 10, (c) 15, and (d) 20 kV. The distance between the spinneret tip and the collector was fixed at 10 cm, and the weight ratio of the inorganic to PVA was 18%.

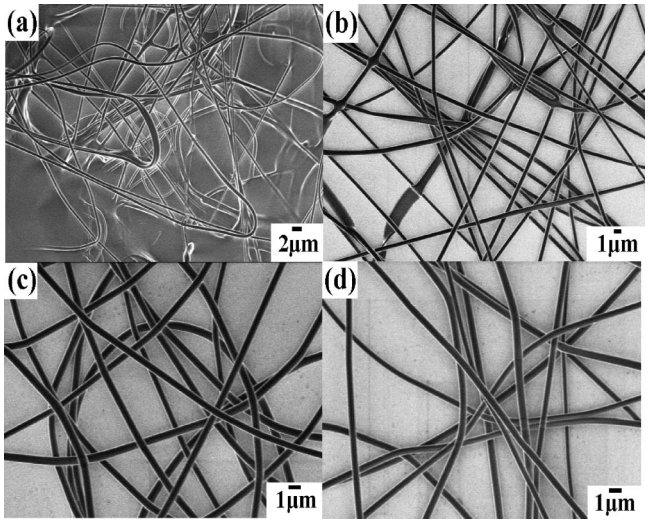

Figure 3. FE-SEM images of the precursors fibers of $YBO_3:Eu^{3+}$ prepared at different distances between the spinneret tip and the collector: (a) 10, (b) 15, (c) 20, and (d) 25 cm. The applied voltage was fixed at 15 kV, and the weight ratio of the inorganic to PVA was 18%.

samples were placed into a liquid nitrogen cycling system (pellet). A continuous 325 nm light from a He−Cd laser was used as the excitation source. The spectra were recorded by a UV-Laboratory Raman Infinity with a resolution of 2 cm^{-1}.

Results and Discussion

(A) Morphology of the Precursor Fibers on Electrospinning Conditions. Changing the electrospinning conditions, such as the distance between the spinneret tip and the collector, the applied voltage and the content of the precursors, have a large influence on the size and morphology of the precursor fibers of $YBO_3:Eu^{3+}$. It is important to find an optimum electrospinning condition. Figures 2–4 depict the FE-SEM images of the precursors fibers prepared under different conditions (changing the applied voltage, the distance between the spinneret tip and the collector and the

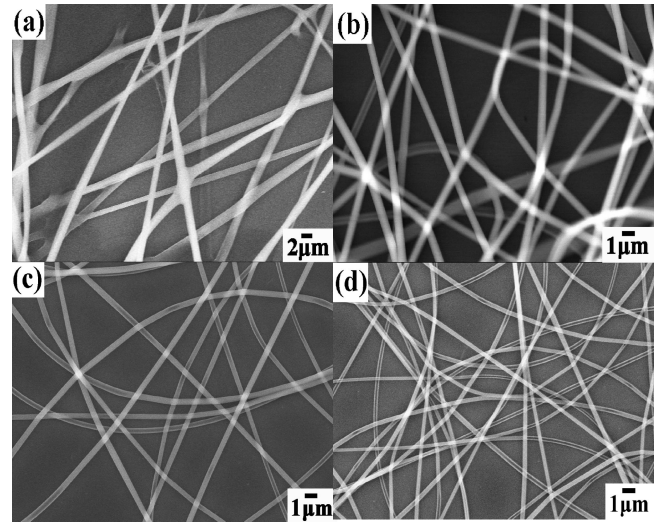

Figure 4. FE-SEM images of the precursors fibers of $YBO_3:Eu^{3+}$ prepared at different weight ratios (a) Inorganic/PVA=0.72; (b) Inorganic/PVA=0.36; (c) Inorganic/PVA=0.23; (d) Inorganic/PVA=0.18. The applied voltage was10 kV and the distance between the spinneret tip and the collector was 20 cm.

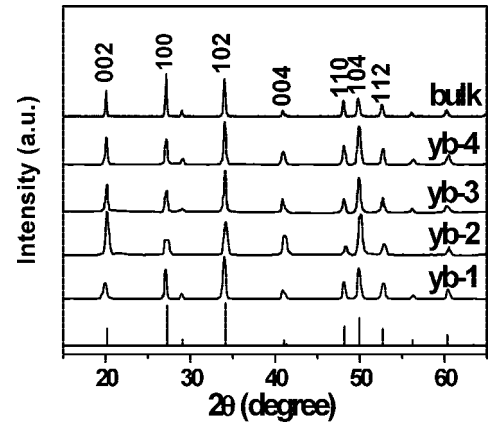

Figure 5. XRD patterns of the $YBO_3:Eu^{3+}$ nanocrystalline fibers as well as the bulk. In the figure, yb1, yb2, yb3, and yb4 correspond to the samples prepared by inorganic/PVA = 0.72, 0.36, 0.23, and 0.18, respectively.

ratio of inorganic precursor to PVA). Accordingly, it can be concluded that homogeneous fibers of diameters 0.5−2.0 μm were obtained when the applied voltage was in the range of 5−15 kV. Varying the applied voltage within this range had no obvious influence on the diameter of fibers. When the applied voltage was increased to 20 kV, the fibers prepared became inhomogeneous. When the distance from the spinneret was too small (<5 cm), the fibers was adhesive. As the distance increased (>10 cm), the fibers did not stick to each other. In the studied range, an increase of inorganic contents to PVA caused the diameter of the precursor fibers to increase gradually, varying from 0.5 to 2.0 μm.

(B) Morphology and Structure of the $YBO_3:Eu^{3+}$ Nanocrystalline Fibers. After being annealed, the PVA content was removed from the precursor fibers and $YBO_3:Eu^{3+}$ nanofibers were formed. Figure 5 shows the powder XRD patterns of the nanocrystalline $YBO_3:Eu^{3+}$ after annealing in contrast to the bulk and the standard card of YBO_3. It can be seen that the nanocrystalline fibers as well as the bulk $YBO_3:Eu^{3+}$ crystallized in the pure hexagonal phase, with all of the expected diffraction peaks in JCPDS

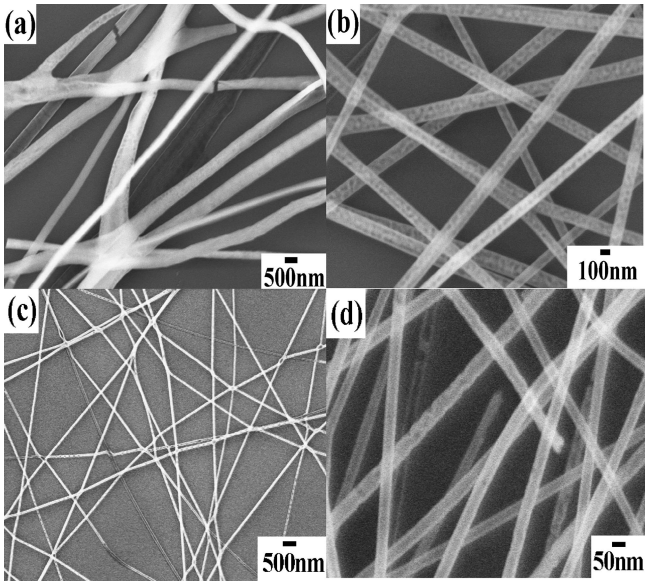

Figure 6. FE-SEM images of the nanofibers of $YBO_3:Eu^{3+}$ after annealing, corresponding to the precursor fibers in Figure 4: (a) inorganic/PVA = 0.72; (b) inorganic/PVA = 0.36; (c) inorganic/PVA = 0.23; (d) inorganic/PVA = 0.18.

card (No. 13−0531). The peak positions in the XRD patterns of the nanofibers are nearly the same as those in the bulk. In comparison to the standard card, the XRD patterns have a slight shift to smaller angles, implying that the unit-cell parameters in europium-doped powders increase by a small amount because of the doping of europium. For instance, the XRD peaks of the (100) and (102) planes locate, respectively, at $2\theta = 27.15$ and 34.01^o for the yb4 and the bulk powders, whereas they locate at $2\theta = 27.27$ and 34.14^o in the standard card. In comparison to the bulk, the XRD patterns become a little bit broader because of a decrease in the crystalline size.

Figure 6a−d shows the FE-SEM images of the $YBO_3:Eu^{3+}$ nanofibers that correspond to the precursor fibers shown in Figure 4. Apparently, after removing PVA, the diameters of fibers decrease greatly. Corresponding to Figure 6a−d, the average diameters of the fibers were determined to be ~500, 130, 80, and 40 nm, respectively. For convenience, they will be referred to yb1, yb2, yb3, and yb4, respectively, in the following text. The nanofibers are narrow and their lengths approach tens of micrometers. Different nanowires or nanotubes do not adhere each other, unlike the nanocrystals prepared by wet-chemical techniques.[27–31] It should be noted that a suitable ratio of inorganic to PVA and accurate annealing conditions are important for the formation of uniform, long, and slender $YBO_3:Eu^{3+}$ nanofibers. If the inorganic contents were too much (inorganic/PVA > 1.0), the precursor fibers could not be easily formed. On the contrary, if the inorganic contents were too little (inorganic/PVA < 0.1), the nanofibers would be easily broken during annealing. The slow and gradual increase in annealing temperature helped prevent the nanofibers from breaking and aggregating.

Actually, as the content of the inorganic precursor was little, the $YBO_3:Eu^{3+}$ electrospinning yielded nanotubes instead of nanowires, which was clearly observed by the enlarged FE-SEM images. To reveal the morphology and

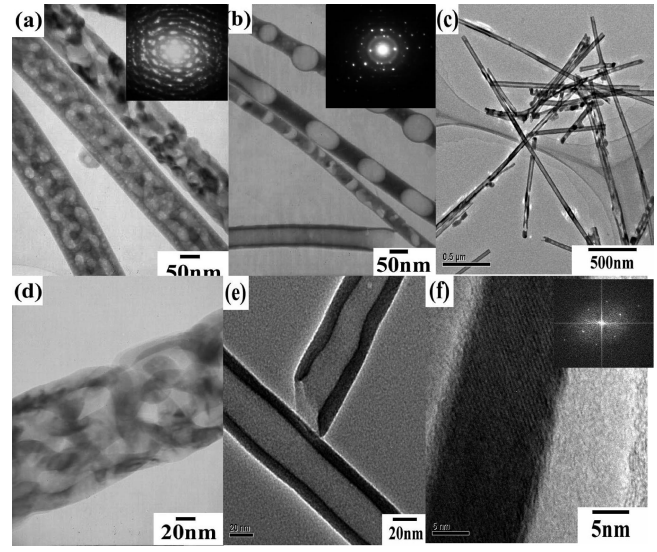

Figure 7. (a) TEM image and SAED patterns (inset) of yb2; (b) TEM image and SAED patterns (inset) of yb3; (c) TEM image of yb4; (d) magnified TEM image of yb2; (e) magnified TEM image of yb4; (f) HR-TEM image and FFT patterns (inset) of a single nanotube in yb4.

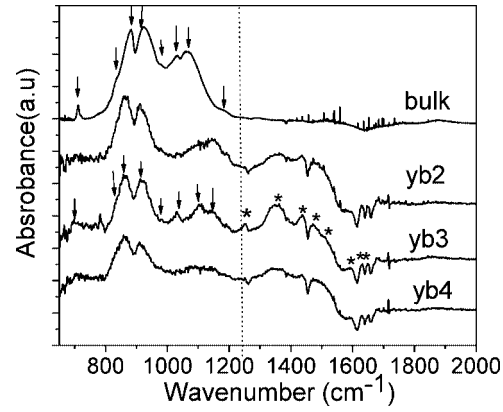

Figure 8. FTIR spectra of the $YBO_3:Eu^{3+}$ electrospinning products in comparison with the bulk.

structure of the $YBO_3:Eu^{3+}$ products further, HR-TEM, SAED, and FFT images of samples yb2, yb3, and yb4 were taken and are shown in Figure 7a−f. It can be seen that the yb2 nanowires contain a large number of holes with a channel structure. The yb3 sample is a mixture of nanowires and nanotubes and the holes became larger in comparison to those in yb2. The yb4 contains nanotubes with an average wall thickness of 5−10 nm and outer diameter of 40 nm. The SAED and FFT patterns all show that the nanotubes or nanowires are single-crystalline (nanotubes) or polycrystalline (nanowires) and in hexagonal phase. Judged from the high-resolution TEM patterns of a single nanotube, it grows along the axis of [110]. The lattice constant c can be deduced to be 9.04 Å, which is a little bit larger than the typical YBO_3 ($a = 6.54$ Å, $c = 8.81$ Å).

Figure 8 compares the FTIR absorption spectra of various $YBO_3:Eu^{3+}$ electrospinning products with the bulk YBO_3. In the bulk, eight absorption bands are observed in the range of 700−1200 cm^{-1}, locating at 709, 837, 883,929, 981, 1030, 1070, and 1181 cm^{-1}, which are in good agreement with those in previous reports. Referring to the IR assignments,[35–38] the bands in the region of 700−950 cm^{-1} are attributed to

the ring stretching vibration modes, whereas the bands in the region of 950−1200 cm^{-1} are attributed to the terminal stretching vibration modes of the $(B_3O_9)^{9-}$ ring groups with boron coordination number of +3. In the electrospinning products, the vibration modes derived from $(B_3O_9)^{9-}$ groups could still be identified. However, the relative intensities of these modes vary considerably in comparison to those of the bulk, which are attributed to the low-dimensional structure as well as the varied coordination environment of the boron atom. In addition, a number of additional vibrational bands appeared in the range of 1200−1400 cm^{-1}, which are attributed to the vibrational modes of $(BO_4)^{5-}$ groups with a boron coordination number of +4.[38] Note that the vibrational bands in the range of 1200−1400 cm^{-1} might originate from the adsorption of $(BO_4)^{5-}$ groups existing in the phase of Y_3BO_6. In the preparation of YBO_3, additional Y_3BO_6 phase can easily form, depending on the preparation conditions, especially the ratio of yttrium to the borate.[39] However, the present vibrational peaks in the range of 1200−1400 cm^{-1} are not accurately consistent with the adsorption of $(BO_4)^{5-}$ groups in the bulk Y_3BO_6 phase. To date, the accurate microstructure of YBO_3 is still unclear. Considerable controversies, mainly concentrating on the space group or site symmetry of cation, are going on.[40] On the basis of the FTIR spectra, we suggest that in the present YBO_3:Eu^{3+} nanowires and nanotubes, the surface coordination environments have changed largely in contrast to the bulk. On the surface of nanowires/nanotubes or the surface of pin holes, a number of $(BO_4)^{5-}$ groups occur in the YBO_3 phase. Note that the existence of an extra phase in the FTIR spectra of the YBO_3 fiber samples are not inconsistent with the result of XRD patterns; the reason being that the former method has higher definition than the latter. Actually, as the extra phase is less than 1−2% of the conventional phase, it is hard to detect in the XRD patterns.

To identify structural defects, ESR experiments were performed on the YBO_3:Eu^{3+} nanofibers and compared with those of the bulk. The comparison is shown in Figure 9. In the YBO_3: Eu^{3+} nanotubes, a weak signal between 3000 and 3500 Guass is observed, which is hardly observable in the bulk powders. The signal is asymmetrical and has a hollow around 3300 Gauss. It is assigned to unshared electron pair of nanocrystalline YBO_3, i.e., surface state of nanocrystalline YBO_3. According to the width and shape of the signal, we suggest that it originates from transition metal ions. Noted that a similar ESR signal was also observed in nanocrystalline Y_2O_3 powders prepared by solution combustion.[41] The signal was attributed to the surface dangling bonds of yttrium. The existent of dangling bonds of yttrium means the existence of corresponding oxygen vacancies in the nanocrystals. This

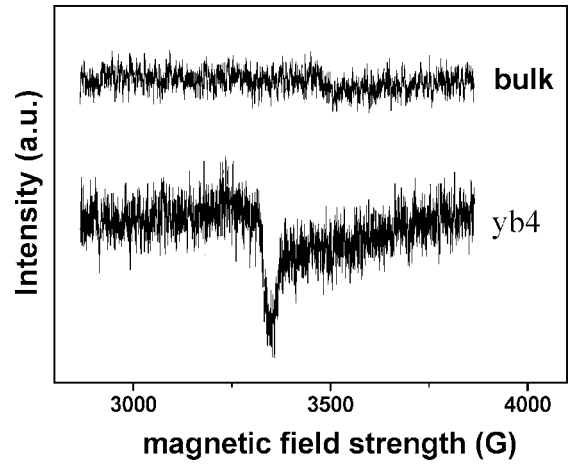

Figure 9. ESR spectra of the YBO_3:Eu^{3+} electrospinning products (yb4) in comparison with the bulk.

will be further proved by the following photoluminescence studies. The forming of surface dangling bonds should be related to the preparation method. As described, the YBO_3 nanocrystals were formed with the volatilization of PVA existed in the precursor nanofibers. The covalent oxygen in PVA might adsorb yttrium ions in the precursor. In the volatilization, some yttrium ions would be inevitably dissolved together with PVA, leading to the formation of dangling bonds on the surface of the nanotubes or the pin holes.

(C) Photoluminescence Properties. To better understand the relationship between photoluminescence and structure, the photoluminescence properties of the YBO_3: Eu^{3+} nanowires and nanotubes, including energy transfer, electronic transition and relaxation, and thermal quenching, were systemically studied in contrast to the bulk. Figure 10a depicts the general excitation spectra of various YBO_3: Eu^{3+} samples. In the excitation spectra, the band in the range of 200−280 nm is assigned to the charge transfer (CT) transition of Eu^{3+}, and the weak lines in the range of 310−340 nm to the $^7F-^5H$ inner-shell transition of Eu^{3+}. The location of the CT transition is at 240 nm (5.17 eV) in the bulk, and it blue shifts to 234 nm (5.30 eV) in the nanotubes and nanowires. The CT band corresponds to the electronic transition from the 2p orbital of O^{2-} to the 4f orbital of Eu^{3+}, and is related closely to the covalency between O^{2-} and Eu^{3+} and coordination environment around Eu^{3+},[42,43] The increase in energy for electron transfer in O^{2-} to Eu^{3+} represents the decrease in the covalency between oxygen and Eu^{3+}. Note that the variation of the CT band described in different literatures is quite incompatible. For example, in Y_2O_3:Eu^{3+} nanocrystals, some authors observed a blue shift whereas the others observed a red shift.[42,44]

In the emission spectra (see Figure 10b), three $^5D_0-^7F_J$ lines were observed, locating at 591, 609, and 624 nm, respectively. The $^5D_0-^7F_1$ peak at 591 nm is dominant, like that in bulk powders. In the nanocrystals, the intensity ratio of the electric-dipole $^5D-^7F_2$ transition to magnetic-dipole

(35) Laperches, J. P.; Tarte, P. *Spectrochim. Acta* **1966**, *22*, 1201.
(36) Kriz, H. M.; Bray, P. J. *J. Chem. Phys.* **1961**, *51*, 3624.
(37) Denning, J. H.; Ross, S. D. *Spectrochim. Acta A* **1972**, *28*, 1775.
(38) Chadeyron, G.; Ghozzi, M. E.; Mahiou, R.; Arbus, A.; Cousseins, J. C. *J. Solid. State. Chem.* **1997**, *128*, 261.
(39) Yu, Z.; Huang, X.; Zhuang, W.; Cui, X.; Li, H. *J. Alloys Compds.* **2005**, *390*, 220.
(40) Lin, J.; Sheptyakov, D.; Wang, Y.; Allenspach, P. *Chem. Mater.* **2004**, *16*, 2418.
(41) Wang, J. W.; Song, H. W.; Sun, B. J.; Ren, X.; Chen, B. J.; Xu, W. *Chem. Phys. Lett.* **2004**, *379*, 501.
(42) Igrashi, T.; Ihara, M.; Kusunoki, T.; Ohno, K. *Appl. Phys. Lett.* **2000**, *76*, 1549.
(43) Li, L.; Zhang, S. Y. *J. Phys. Chem. B* **2006**, *110*, 21438.
(44) Qi, Z.; Shi, C.; Zhang, W.; Hu, T. *Appl. Phys. Lett.* **2002**, *81*, 2857.

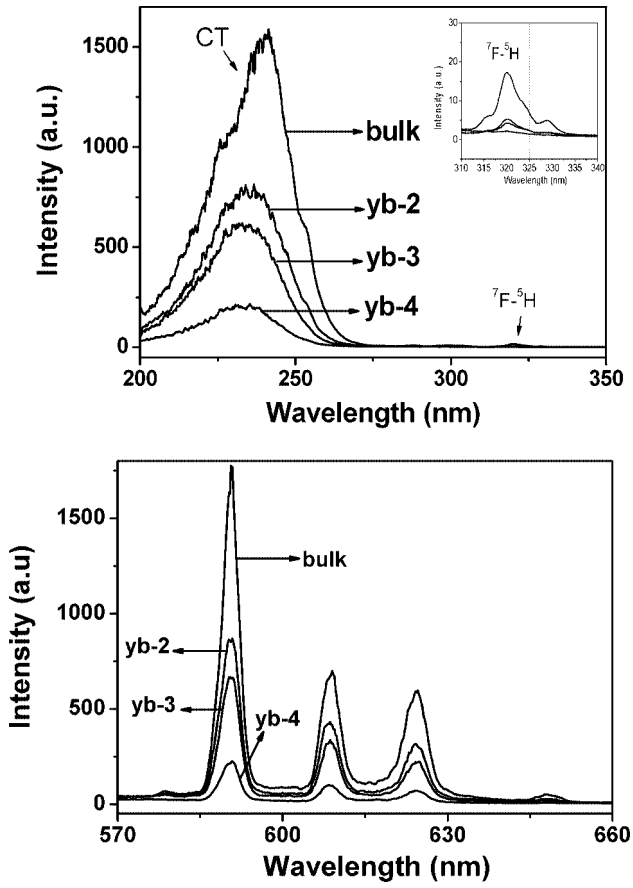

Figure 10. (a) Excitation ($\lambda_{em} = 591$ nm) and (b) emission ($\lambda_{ex} = 245$ nm) spectra of various $YBO_3:Eu^{3+}$powders.

$^5D_0-^7F_1$ transition has a little increase in contrast to that in the bulk (the intensity ratios of $I(^5D_0-^7F_2)/I(^5D_0-^7F_1)$ were deduced to be 0.39, 0.50, 0.50, and 0.45, respectively, in the bulk, yb2, yb3, and yb4). In the $YBO_3:Eu^{3+}$ nanocrystals prepared by the hydrothermal method and sol−gel method, some authors observed that the red $^5D_0-^7F_2$ emission increased greatly relative to the orange $^5D-^7F_1$ emission; as a consequence, the color purity of the red was greatly improved.[28,29] The present result suggests that in the previous references the considerable increase of $I(^5D_0-^7F_2)/I(^5D_0-^7F_1)$ in nanocrystals probably originated from decreased site symmetry induced by worsen crystallinity in comparison to the bulk. According to the excitation and emission spectra, it can also be concluded that in the $YBO_3:Eu^{3+}$ products, the brightness for the $^5D_0-^7F_J$ emissions of Eu^{3+} decreased in contrast to the bulk, like that in the other nanocrystalline systems. This is because of the nonradiative energy transfer from charge transfer states to surface defect states. Further work should be performed to decrease the surface defect states involved in the sample preparation.

The fluorescence decay curves of the $^5D_0-^7F_2$ emissions of Eu^{3+} ions under 266 nm excitation were measured at room temperature. The results demonstrate that the fluorescence decayed nearly exponentially for all the samples. The exponential lifetimes for the $^5D_0$ states are found to be 2.69, 2.08, 1.93, and 1.63 ms for the bulk, yb2, yb3, and yb4. Apparently, the fluorescence lifetimes for the $^5D_0$ state in $YBO_3:Eu^{3+}$ nanocrystals gradually become shorter with the decreasing diameter. In some literature, the fluorescence lifetime for Eu^{3+} decreased with particle size,[45,46] on the contrary, in the other literature, the lifetime increased, which depended on the host and the preparation method, etc.[47,48] The increase in fluorescence lifetime in the nanocrystals was mainly attributed to the influence of refractive index,[49] whereas the decrease of florescence lifetime was generally attributed to the increased nonradiative rate due to the energy transfer from excited states of rare earth ions to surface defect states.[45,46] Our previous quantitative studies on cubic $Y_2O_3:Eu^{3+}$ nanocrystals prepared by combustion demonstrated that in the nanocrystals the electronic radiative transition rate for Eu^{3+} also increased a little due to the lattice distortion.[45,46] Related to the variation of fluorescence lifetime in nanocrystals, further experimental and theoretical works should be performed.

Conclusions

A simple electrospinning method was explored to prepare single-distributed one-dimensional $YBO_3:Eu^{3+}$ nanocrystals, for the first time to the best of our knowledge. The diameters of the obtained $YBO_3:Eu^{3+}$ nanowires and nanotubes depend strongly on weight ratio of inorganic materials to PVA in electrospinning solutions, varying from 40 to 500 nm. The nanowires and nanotubes yield single crystals or quasi-single-crystals and are hexagonal in phase. The FTIR and ESR spectra indicate that the coordination environments of the nanowires and nanotubes changes greatly in comparison to the bulk because of the existence of a number of surface dangling bonds. The luminescence properties of the $YBO_3:Eu^{3+}$ nanowires and nanotubes were also studied in contrast to the bulk powders. Overall, electrospinning is a novel and effective technique for fabricating one-dimensional nanostructure luminescence materials, especially for those that cannot be easily prepared through other methods.

Acknowledgment. H.S. thanks the financial support by the National Natural Science Foundation of China (Grants 55772042, 10704073, and 10504030) and the National Key Project of China (Grant 2007AA03Z314).

CM8007864

(45) Peng, H. S.; Song, H. W.; Chen, B. J.; Wang, J. W.; Lu, S. Z.; Kong, X. G. *J. Chem. Phys.* **2003**, *118*, 3277.
(46) Song, H. W.; Wang, J. W.; Chen, B. J.; Lu, S. Z. *Chem. Phys. Lett.* **2003**, *376*, 1.
(47) Williams, D. K.; Bihari, B.; Tissue, B. M. *J. Appl. Phys.* **2001**, *90*, 3516.
(48) Williams, D. K.; Yuang, H.; Tissue, B. M. *J. Lumin.* **1999**, *83−84*, 297.
(49) Meltzer, R.; Feofilov, S.; Tissue, B. M. *Phys. Rev. B* **1999**, *60*, R14012.